Desalination 496 (2020) 114731

Contents lists available at ScienceDirect

Desalination

journal homepage: www.elsevier.com/locate/desal

Improved performance of thin-film composite forward osmosis membrane with click modified polysulfone substrate

Hasan Salehi[a], Alireza Shakeri[a,*], Hossein Mahdavi[a], Rob G.H. Lammertink[b,**]

[a] School of Chemistry, College of Science, University of Tehran, P.O. Box 14155-6619, Tehran, Iran
[b] Soft matter, Fluidics and Interfaces, Membrane Science and Technology, MESA + Research Institute, University of Twente, P.O. Box 217, NL-7500 AE Enschede, the Netherlands

GRAPHICAL ABSTRACT

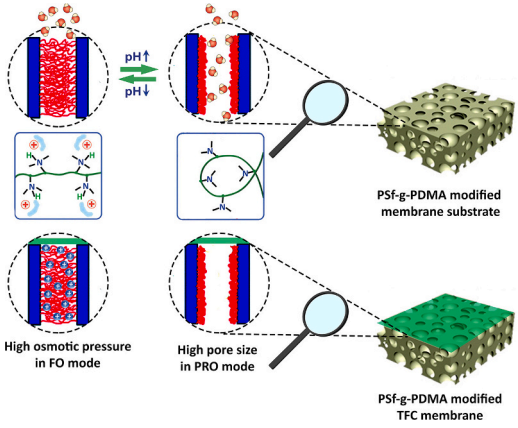

ARTICLE INFO

Keywords:
Graft copolymer
pH-responsive
Substrate polymer
Forward osmosis
Click chemistry
Thin film composite membrane

ABSTRACT

In this study, polysulfone-graft-poly(2-dimethylaminoethyl methacrylate) (PSf-g-PDMA) as a pH-responsive graft copolymer was synthesized for the first time via a combination of click chemistry and atom transfer radical polymerization (ATRP). This graft copolymer was blended with polysulfone during the phase inversion. The so formed substrate was used for the fabrication of a forward osmosis (FO) membrane via interfacial polymerization. The influence of the copolymer concentration on hydrophilicity, morphology, porosity, FO performance, and TFC layer characteristics were thoroughly investigated using diverse analysis. To prove pH-sensitivity of the PSF-g-PDMA blended substrate, the pure water permeability (PWP) of substrate containing 10.0 wt% of PSf-g-PDMA copolymer (G_{10}) was measured at different pH values (3.0–12.0). As the pH of the feed solution was changed from 3.0 to 12.0, the PWP increased from 221.3 to 299.4 LMH/bar. In addition, the performance of PSF-g-PDMA based TFC membrane in FO process was studied. Compared to the pure PSf based TFC membrane, the PSf-g-PDMA modified TFC-FO membranes demonstrated increased water flux without adversely affecting their selectivity. In addition, the TFC-G_{10} membrane exhibited a reversible pH-dependence water flux. The pH-reversibility was investigated using draw solution with different pH values (3.0 and 10.0) where acidic draw solutions show higher water fluxes than basic draw solutions.

* Correspondence to: A. Shakeri, P.O. Box 14155-6619, Tehran, Iran.
** Correspondence to: R.G.H. Lammertink, P.O. Box 217, NL-7500 AE Enschede, the Netherlands.
E-mail addresses: alireza.shakeri@ut.ac.ir (A. Shakeri), r.g.h.lammertink@utwente.nl (R.G.H. Lammertink).

https://doi.org/10.1016/j.desal.2020.114731
Received 28 July 2020; Received in revised form 24 August 2020; Accepted 27 August 2020

1. Introduction

Nowadays, global scarcity of freshwater and increasing demand for clean water has inevitably become a debating issue in numerous parts of the world [1–3]. Wastewater reuse and seawater desalination play a significant role in solving present and future global water problems [4]. Separations of freshwater from other impurities using today's technology is expensive and energy-intensive; so there is a critical need for design, development, and implementation novel technologies to purify water at lower energy, lower cost and prominently minimum impact on the environment [5]. Recently, forward osmosis (FO) has attracted intensive interests as a new class of membrane-based separation technologies due to their outstanding advantages such as high water flux, efficient contaminant rejection, low energy consumption and low fouling tendency [6–9]. Despite that, the deficiency of membrane is one of the serious challenges which hamper the progress of FO technology [10–12]. The dominant FO membrane concerns a thin film composite (TFC) membrane which consists of an asymmetric structure with a porous support layer prepared via phase inversion method and a thin selective film prepared by interfacial polymerization (IP) [13–15]. The efficiencies of FO processes (water flux) are mainly controlled by the membrane substrate characteristics, particularly by tortuosity, porosity, morphology and hydrophilicity [16–18]. Internal concentration polarization (ICP) has been one of the most general and unavoidable phenomena in FO processes [19,20]. The ICP degree is mainly determined by the chemical and structural properties of the membrane substrate, which can be determined quantitatively by the S value (S = tortuosity × thickness/porosity) [21,22]. For a successful FO process, a small S value is needed to guarantee a low transport resistance and minimize the ICP effect in the membrane substrate [23–25]. Thus, a thin, hydrophilic and porous substrate with adequate chemical, mechanical, and thermal stability are preferred for high water flux TFC-FO membranes [19,26,27]. Since the membrane substrate also has an important role in the growth of the PA layer via IP reaction, the modification of the membrane substrate is, therefore, greatly beneficial to FO process efficiency [28].

In recent decades, developments have been reported on the substrate modification to alleviate ICP effect of TFC-FO membranes, through the blending of hydrophilic components [29], surface modification [30], nanomaterial incorporation [31], or template-assisted techniques [32]. Among them, membrane formation from a mixture of base membrane polymer and hydrophilic species is the common modification strategy of TFC-FO membranes [33–35]. Unfortunately, most of the membrane prepared by these traditional hydrophilic additives usually has nonadjustable water permeability that can hinder their applications in water treatment fields. In contrast, environmental stimuli-responsive membranes allow some control over the pore sizes according to an external stimulus [36]. Fabrication of these stimuli-responsive membranes is of both technological and scientific interest. These membranes are mostly fabricated by introduces of stimuli responsive species during membrane formation using a blend containing of a membrane-forming polymer along with stimuli responsive species [37]. This approach shows great potential for scale-up in practical applications by using conventional membrane preparation techniques [38,39].

For the first time, in this study, we synthesize a new PSf based graft copolymer, polysulfone-*graft*-poly(2-dimethylaminoethyl methacrylate) (PSf-g-PDMA), as a potential additive for fabricating hydrophilic and pH-sensitive TFC-FO membrane. PSf was chosen as the main polymer chain to increase the miscibility of copolymer with the membrane matrix while PDMA was used as graft because of its various characteristics such as: (1) fast response to external stimuli such as the pH, (2) versatile synthesis strategies, (3) high hydrophilicity and (4) high flexibility. While various additive and fillers such as hydrophilic polymers and nanoparticles have been used to modify porous substrates of TFC-FO membranes, the use of pH-responsive and amphiphilic graft copolymer to prepare hydrophilic and smart TFC membranes is a novel strategy. It is expected that the water permeability of membranes modified by this additive graft copolymer displays a response to the pH of the feed solution.

2. Experimental methods

2.1. Materials

Polysulfone (PSf, Ultrason S6010) was provided by BASF and used as membrane substrate polymer. Meanwhile, paraformaldehyde (96%), tin (IV) chloride ($SnCl_4$, 99%), sodium azide (NaN_3), chlorotrimethylsilane ($(CH_3)_3SiCl$, 99%), and chloroform ($CHCl_3$) were purchased from Merck company and used for synthesis of chloromethylated and azide functionalized polysulfone. α-bromoisobutyryl bromide (BIBB), dichloromethane (CH_2Cl_2, DCM) and propargyl alcohol for synthesis of ATRP initiator, 2-(Dimethylamino)ethyl methacrylate (DEMA, 98%) as monomer, copper (I) chloride (CuCl, 99%) as catalyst, *N*,*N*,*N*′,*N*′,*N*″-pentamethyl diethylene triamine (PMDETA, 98%) as ligand, *N*-methyl-2-pyrrolidone (NMP, 98%) and *N*,*N*-dimethylformamide (DMF, 98%) as solvents in ATRP reaction were obtained from Merck Chemical Co. Trimesoyl chloride (TMC, 98%, Merck) and *m*-phenylenediamine (MPD, > 99%) were used as the active monomers to form PA active layers. n-hexane (99%, Merck) and distilled water were used as TMC and MPD solvent, respectively. In FO performance tests, NaCl (Iran Mineral Salt Company) was used to prepare draw solution.

2.2. Synthesis of chloromethylated PSf

The chloromethylated PSf was synthesized following the literature procedure [40]. Briefly, 15.0 g of PSf was dissolved in 500 ml of chloroform under stirring at 45 °C, when PSf was completely dissolved, 0.25 ml of $SnCl_4$, 10.0 of paraformaldehyde and 35 ml of $(CH_3)_3SiCl$ were slowly added to the above solution. After the mixture was stirred for 3 days at 50 °C, it was precipitated in ethanol to remove the solvent and unreacted reagents. The precipitate was collected by filtration and purified by repeated the dissolution–precipitation process for several times. The final product was collected by filtration and dried at 50 °C for 24 h. Chloromethylated PSf in white powder was obtained and designated with CPSf. Degree of substitution (DS), which represents the average number of chloromethyl groups attached per repeat unit of polymer was calculated by ^{1}H NMR characterization and obtained 0.55.

2.3. Synthesis of PSf-N_3

PSf-N_3 was synthesized by nucleophilic reaction of NaN_3 with chloromethyl groups of CPSf, following the literature procedure along with minor modifications [41]. Firstly, 5 g of CPSf was dissolved in DMF (120 ml) with stirring. Next, 1.60 g of sodium azide was added to the reaction mixture. After stirring for 24 h at 60 °C the mixture was precipitated out using methanol–water (4/1) non-solvent. The precipitate was dried under vacuum at 25 °C for two days.

2.4. Synthesis of initiator

The propargyl-2-bromoisobutyrate (PBiB) was synthesized by the esterification reaction following the literature procedure [42,43]. In summary, propargyl alcohol (11.2 g, 0.20 mol) and triethylamine (33.4 ml, 0.24 mol) were added in 80 ml pre-cooled DCM. Then, BIBB (29.6 ml, 0.24 mol) in DCM solution (40 ml) was added to the mixture dropwisely under stirring for 1 h. After stirring in room temperature for 24 h vacuum filtration was used to remove the insoluble ammonium salts. Finally, the solvent was removed by a rotary evaporator to obtain a colorless liquid. ^{1}H NMR (500 MHz, $CDCl_3$, d, ppm): 1.9 (6H, -$C(CH_3)_2$Br). 2.5 (1H, HC-), and 4.7 (2H, - O CH_2) (Fig. 1).

Synthesis of alkynyl poly(2-dimethylamino)ethyl methacrylate (*alkynyl*-PDMA).

In a typical experiment, 15.7 g of DMA (100 mmol) was added in 10 ml of IPA solvent and degassed. Under an argon atmosphere, CuBr (0.07 g, 0.5 mmol) and PBIB (0.21 g, 1 mmol) were successively added. Then, 0.17 g of PMDETA (1 mmol) as ligand was added to the mixture before sealing the flask with a rubber septum under an argon atmosphere. After 12 h reaction at 80 °C, ATRP reaction was finished by exposing to air. Then a column of neutral alumina removed the catalysts complex, and residual diluted in THF and precipitated out using cold n-hexane. The resulting *alkynyl*-PDMA as a white polymer was dried in a vacuum for 24 h at room temperature. The degree of polymerization (DP) of *alkynyl*-PDMA was calculated to be 30 by ^{1}H NMR analysis in D_2O.

2.5. Synthesis of the PSf-g-PDMA graft copolymer via click reaction

The PSf-g-DMA graft copolymer was synthesized by azide-alkyne click reaction as shown in Fig. 2. About 1 g of PSf-N_3 was dissolved in 30 ml DMF at 80 °C. After cooling down to room temperature, 0.05 g of CuCl as catalyst and 1 g of *alkynyl*-PDMA as graft polymer were added into the above solution. Then, 0.08 g of PMDETA as ligand was added to the mixture before sealing the flask with a rubber septum under an argon atmosphere. The solution was then aged 3 days under continuous stirring at room temperature. Then polymer precipitated out using methanol as non-solvent. The as-prepared graft copolymer was dried under vacuum at 25 °C for two days and represented as PSf-g-PDMA.

2.6. Preparation of the porous membrane substrates

To prepare PSf-g-PDMA blend solution, PSf-g-PDMA graft copolymer was firstly dissolved in NMP solvent. Then, the predetermined amount of PSf polymer was added into the PSf-g-PDMA/NMP solution with a continuous stirring for 5 h at 60 °C, and left overnight to release air bubbles. A casting knife set at the gate height of 100 μm was employed to prepare membrane substrates via phase inversion. The as-prepared membrane substrates were denoted by G_X, where X represents the weight concentration of PSf-g-PDMA copolymer (Table 1).

2.7. TFC membranes preparation

Conventional IP method was used for synthesis of PA layer. First, 2.0 wt% MPD/aqueous solution was gently poured on the top of substrates fixed in a custom-made frame. After 2 min, using a filter paper the residual droplets gently wiping out from the substrate surface. In the next step, a 0.1 wt% TMC/hexane solution was introduced via careful pouring on the top surface of the substrate for 90 s. Finally, the resulting membrane was post-cured in an oven at 60 °C for 1 min.

2.8. Copolymer characterization

Characterization of chemical composition of synthesized copolymer in chloromethylation, azide functionalization reaction, ATRP and click reaction was carried out by using an attenuated total reflectance Fourier transform infrared spectrometer (ATR-FTIR, Bruker, Equinox 55). In addition, ^{1}H NMR spectra of polymer samples were obtained using a Bruker Co., Germany 500 MHz NMR spectrometer. Thermogravimetric analysis (TGA) of polymers was carried out under nitrogen atmosphere with a heating rate of 10 °C/min using Q5000IR (TA instruments, USA).

2.9. Membrane characterization

Changes in the chemical composition of copolymer blended support layer before and after formation of polyamide active layer were investigated over the range of 600–4000 cm^{-1} using ATR-FTIR, Bruker, Equinox 55. In order to observe the top, bottom and cross-section morphology of blended membrane substrate also the top and cross-

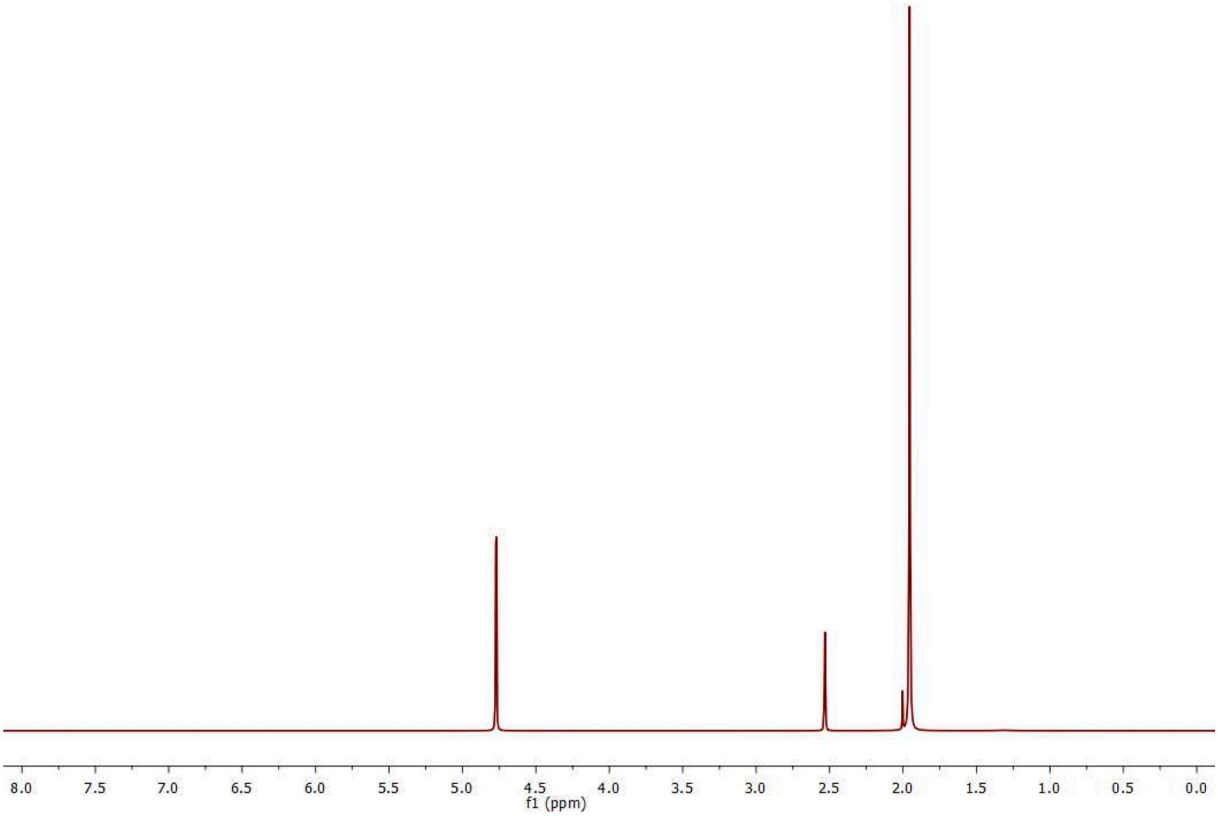

Fig. 1. ^{1}H NMR spectra of PBIB.

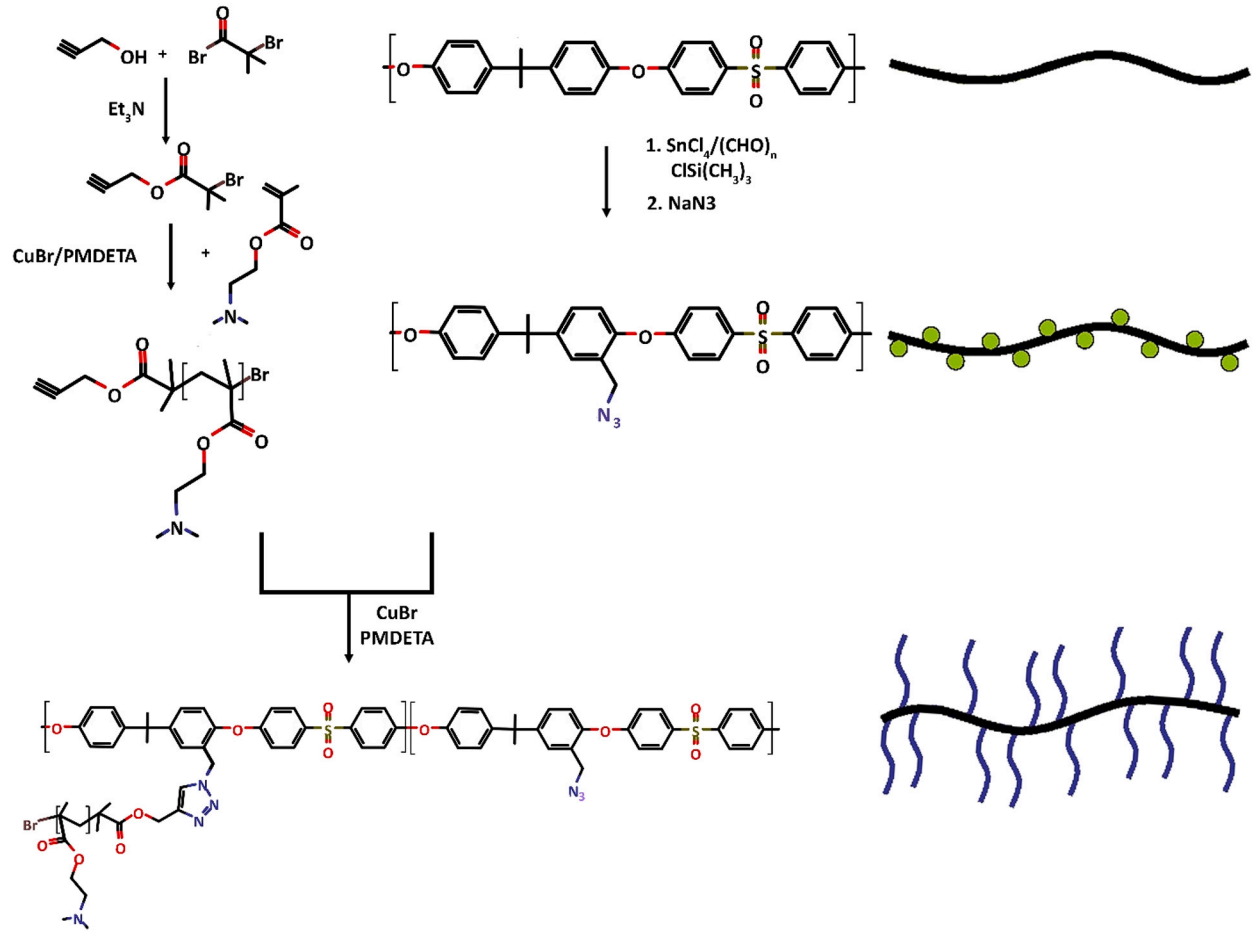

two days and represented as PSf-g-PDMA.

Fig. 2. PSf-g-PDMA copolymer synthesis procedures.

Table 1
PSf/PSf-g-PDMA substrates and corresponding TFC membranes.

Membranes	Polymer		NMP (%)	Corresponding TFC membrane
	PSf (%)	PSf-g-PDMA (%)		
G_0	100	0	85	TFC-G_0
G_5	95	5	85	TFC-G_5
G_{10}	90	10	85	TFC-G_{10}
G_{15}	85	15	85	TFC-G_{15}

section morphology of PA film in TFC membrane, a scanning electron microscope (SEM, Zeiss, DSM 960 A, Germany) was used. For observation the cross-sectional images, prior to gold coating the membrane were fractured in liquid nitrogen. The effect of copolymer blending on hydrophilicity of membrane substrate was estimated by contact angle analysis (Dataphysics, OCA 15 plus) using DI water as liquid test at room temperature to get the water contact angle (WCA). Finally, using atomic force microscopy (AFM, ENTEGRA AFMNT-MDT), the surface topography of the PA layer was examined in tapping-mode.

Membrane substrate porosity (ε) was measured using gravimetric method using following Eq. (1).

$$\varepsilon = \frac{(m_1 - m_2)/\rho_W}{(m_1 - m_2)/\rho_W + m_2/\rho_P} \quad (1)$$

where m_1 and m_2 represent the weight of support layer in wet and dry state respectively, also ρ_p and ρ_w are the density of polymer and water, respectively.

2.10. Pure water permeability tests

Water permeability of membrane substrates at different pH values was measured by a dead end stirred filtration cell that had an effective surface area of 3.14 cm^2. All of the membrane filtration test were performed at room temperature and a pressure of 2.0 bar. The pure water permeability (PWP, LMH/bar) was calculated by the following Equation:

$$PWP = \frac{V}{A_m \times \Delta t} \quad (2)$$

where V, A and t represent the volume of the permeate (L), membrane surface area (m^2), and filtration time (h), respectively.

The mean pore diameter (r_m, nm) of membrane substrates was calculated by the Guerout-Elford-Ferry Equation [44]:

$$r_m = \sqrt{\frac{(2.9 - 1.75\varepsilon) \times 8Q\mu t}{\varepsilon \times A_m \times \Delta P}} \quad (3)$$

where t is membrane thickness (μm), Q is water flux ($m^3 s^{-1}$), μ is water viscosity (Pa.s) and ΔP is hydraulic pressure (Pa).

2.11. Evaluation the interstice separation properties of blended membrane

In order to evaluation the intrinsic separation properties (i.e. water and salt permeability) of TFC membranes a bench-scale RO filtration

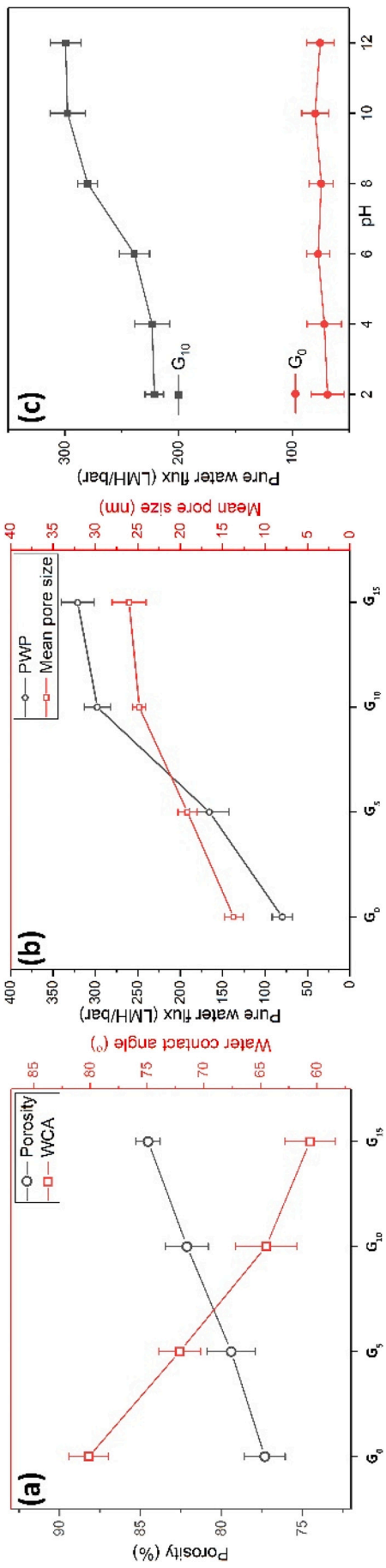

Fig. 3. (a) Porosity and contact angles (values are averages of at least 3 random spots from each membrane sample), (b) pure water permeability and mean pore size of neat and modified membrane substrates, and (c) pH-dependence pure water permeability of G_0 and G_{10} membrane substrates (results are an average of three different membrane coupons).

set-up was used. All RO measurements were performed at room temperature under 5.0 bar hydraulic pressure. The pure water permeability values of membranes were measured by carrying out the experiment using DI water and the following Eqs. (4) and (5):

$$J = \frac{\Delta V}{A_m \times \Delta t} \tag{4}$$

$$A = \frac{J}{\Delta P} \tag{5}$$

where ΔV, A_m, Δt, and Δp represent the volume change of permeate, the effective surface area of flat sheet membrane, the test time, and the trans-membrane hydraulic pressure, respectively.

Knowing the salt concentration in feed side (1000 ppm of NaCl solution, C_f) and permeate solution (C_p), the salt rejection of every TFC-FO membrane (R_s) was eventually measured as following Eq. (6):

$$R_s = \left(1 - \frac{C_p}{C_f}\right) \times 100 \tag{6}$$

By using the solution-diffusion theory salt permeability (B) was measured according to the following Eq. (7) [45]:

$$\frac{1 - R_s}{R_s} = \frac{B}{A(\Delta P - \Delta \pi)} \tag{7}$$

2.12. FO performance test

Water flux and reverse salt flux as FO performances factor of blended membrane were evaluated in a bench-scale FO set-up. All measurements were performed with DI water and 1 M NaCl aqueous solution as draw and feed solutions, respectively, and flow rate of both feed and draw solution was fixed on 100 ml/min in each side. The water flux (J_v, LMH) and reverses salt flux (J_s, gMH) for each membrane was calculated by the weight and salt concentration change of the feed solution according to Eqs. (8) and (9):

$$J_w = \frac{\Delta V}{A_m \Delta t} \tag{8}$$

$$J_S = \frac{\Delta (C_t V_t)}{A_m \Delta t} \tag{9}$$

where the weight changes of feed solution over the predetermined testing time (Δt), and area of membrane (4.9 cm^2) represented as ΔV and A_m, respectively. In addition, V_t and C_t are change of volume of water and NaCl concentration in feed side, respectively. The calibrated conductivity meter was conducted to monitor the salt concentration change in feed side.

The S values of membrane substrate as a function of membrane tortuosity (τ), porosity (ε), and thickness (l) was measured according to the Eq. (10):

$$S = \frac{D_s}{J_V} ln \frac{A\pi_D + B}{A\pi_F + J_V + B} \tag{10}$$

where D_s is the solute diffusion coefficient, π_D and π_F are the osmotic pressure at the draw and feed side, respectively.

3. Results and discussion

3.1. Characterization of the PSf-g-PDMA copolymer blended substrate

The PSf-g-PDMA blended PSf membranes were prepared by traditional non-solvent induced phase inversion. The obtained membranes were left in the coagulation bath for 30 min, quickly rinsed with pure water and stored in DI water. To examine the effect of copolymer concentration on the membrane properties, we primarily fixed the total polymer content in the casting solution to 15 wt% while adjusting the

weight ratio of PSf-*g*-PDMA between 0 and 15 wt%.

The porosity and water contact angles of PSf-*g*-PDMA blended membrane substrates with different concentrations are presented in Fig. 3a. In general, membrane substrates with high hydrophilicity and porosity are desired to reduce ICP during FO process [46]. Both the porosity and hydrophilicity increase with the PSf-*g*-PDMA weight ratio. As can be seen, the WCA of blended substrates gradually decreases from 87° for G_0 to 61° for G_{15} with the increase of the PSf-*g*-PDMA weight ratio from 0 to 15 wt%. The major reason of the improved membrane hydrophilicity can be attributed to the presence of hydrophilic PDMA side chains in PSf-*g*-PDMA. Moreover, the improved porosity of the blended membrane substrate may result from the fact that (i) PSf-*g*-PDMA blending decrease the phase inversion rate, or (ii) the modified membranes with high hydrophilicity entirely wet in water, rises the

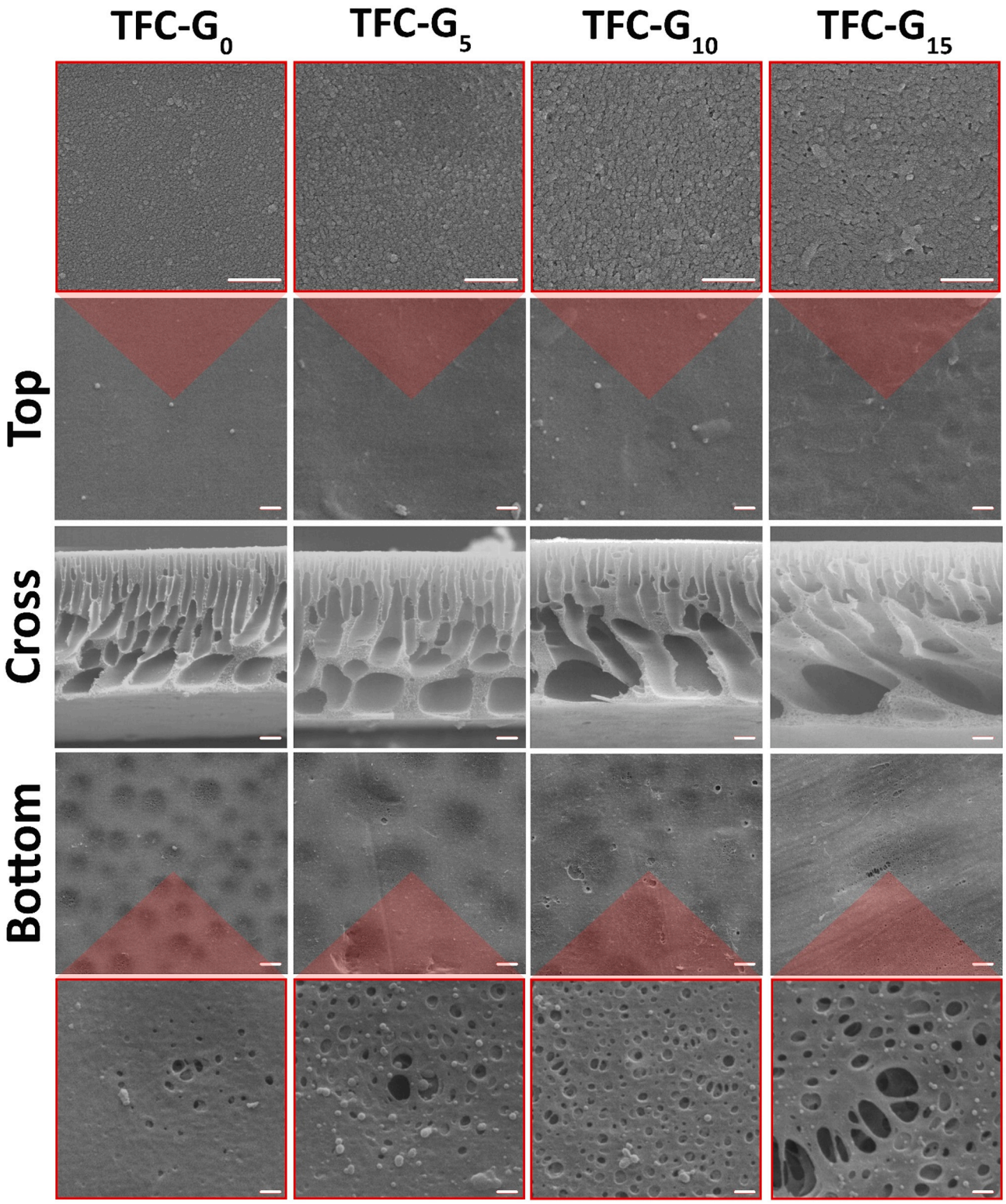

Fig. 4. Top, cross and bottom morphology of different membrane substrates (scale bars are 1, 10 and 10 μm for top, cross and bottom, respectively and 1 μm for magnified images).

effective porosity [18,47]. Moreover, Fig. 4 also shows that the finger-like pores become larger with increasing mass ratio of PSf-*g*-PDMA, which is consistent to the corresponding overall porosity.

The pure water permeability (PWP) of membrane substrates are also measured using a dead-end filtration set-up (Fig. 3b). The PWP value for modified membranes massively increases from 79.9 to 321.1 LMH/bar when the PSf-f-PDMA weight ratio increases from 0 to 15 wt%. Commonly, the membrane permeability depends on the hydrophilicity, porosity and pore diameter of the membrane [6]. The improvement in PWP of the blended membrane substrate results from several factors: (i) large pores and high porosity of modified substrate can enhance the PWP, (ii) high hydrophilic surface in modified substrate tend to drawing water molecules into the substrate and enhancing PWP, (iii) finger-like morphology in modified membrane substrates decrease the water transport pathway significantly.

The pore diameter of membrane substrates was also calculated by the Guerout–Elford–Ferry equation on the basis of the PWP and porosity data [48]. As depicted in Fig. 3b, the pore diameter of the substrate increase with the increase of PSf-*g*-PDMA weight ratio. The increase in the pore diameter could be ascribed to the decreased phase inversion rate with PSf-*g*-PDMA blending.

While the G_0 substrate exhibited a constant PWP 79.9 LMH/bar between pH 2.0 and 12.0, the G_{10} substrate showed pH-responsiveness. As the pH of the feed solution was changed from 2.0 to 12.0, the PWP increased from 221.3 to 299.4 LMH/bar. The pH-responsive PWP behavior of the G_{10} membrane could be attributed to the transition in the conformation of the PDMA polymers on the membrane surface and pore walls. The protonation of dimethylamino (DMA) groups of PDMA polymers (pK_a = 7.5) [49] and repulsion between these positive groups in acidic aqueous solution caused the side chain to extend reducing the effective pore volume. At high pH value, the DMA groups were deprotonated which caused a collapsed conformation and an increased effective pore volume.

The top surface, bottom surface, and cross-section morphology of all pristine and modified membranes were investigated by SEM (Fig. 4). According to the SEM images of top surface, all substrates have a relatively smooth and nanoporous structure. Increasing the PSf-g-PDMA content led to a slight increase in porosity and average diameter of pores. This change in the surface morphology is consistent with the increased PWP of the modified membrane substrates comparative to that of the pristine PSf membrane.

The cross-sectional SEM images of substrates with different concentrations of PSf-g-PDMA are presented in Fig. 4. For the pristine PSf substrate, several finger-like macro voids were divided by a partial sponge-like medium in between. For the PSf-g-PDMA blends with PSf, these macro voids became larger and considerably more irregular. This morphology change of the substrate could be due to the fact that, the PSf-g-PDMA graft copolymer is much more hydrophilic than the PSf homopolymer. Due to its hydrophilicity, PSf-g-PDMA favors the entrance of non-solvent into the membrane which enlarges pore size and overall porosity of modified substrates [44]. As the weight ratio of the graft copolymer increases, the affinity of the casting solution to non-solvent increases, causing a slower exchange rate for solvent and non-solvent during phase separation before solidification. A slower solvent and non-solvent exchange rate favors the formation of larger finger-like pores and suppresses the formation of sponge-like morphology [50,51].

The weight ratio of PSf-g-PDMA has some effect on the bottom surface morphology of graft copolymer blended membrane substrates. As shown in Fig. 4, the increase in weight ratio of PSf-g-PDMA results in a highly porous bottom surface with large pores, while the pure PSf membrane possesses a relatively dense bottom surface. A more porous bottom is estimated to improve the water and solute diffusion across the membrane. Generally speaking, the introduce of PSf-g-PDMA in PSf substrate tends to form a hydrophilic support layer with more favorable finger-like morphology, dense top layer and porous bottom layer.

3.2. Characterizations of the TFC-FO membranes

Fig. 5 shows the top surface and cross-section of PA thin film formed on the PSf and PSf-g-PDMA blended substrates. The top surfaces of all TFC membranes are completely covered by a typical ridge-and-valley morphology, which confirms the successful synthesis of PA layer via IP reaction. The TFC-G_0 membrane has the smoothest surface with a more leaf-like morphology, while the TFC-G_{15} one has the roughest surface with a ridge-and-valley morphology. The size of the PA nodules increases with raising the weight ratio of copolymer, suggesting that the blending of PSf-g-PDMA with PSf affects the formation of PA layer during IP process. The thickness and roughness of the PA layer also increase with an increase in copolymer content. This observation is similar to previously reported works, which found that porous and hydrophilic substrates produced thicker and rougher active layers [23,52,53]. During the IP process, MPD must migrate from the substrate into the organic side and react with TMC to form the active layer. Generally, a substrate with small pore and pore size distribution favors slow mass transfer and produces a smooth and thin PA layer, while a substrate with large pore and pore size distribution has a tendency to form a rough and thick PA layer [54]. The TFC-G_0 membrane has a smoother surface with more leaf-like morphology while the TFC-G_{15} membrane substrate with large pores produces a rougher surface and a ridge-and-valley morphology.

The effect of the PSf-g-PDMA loading on the surface roughness of TFC membranes in terms of root mean square (R_q) and average

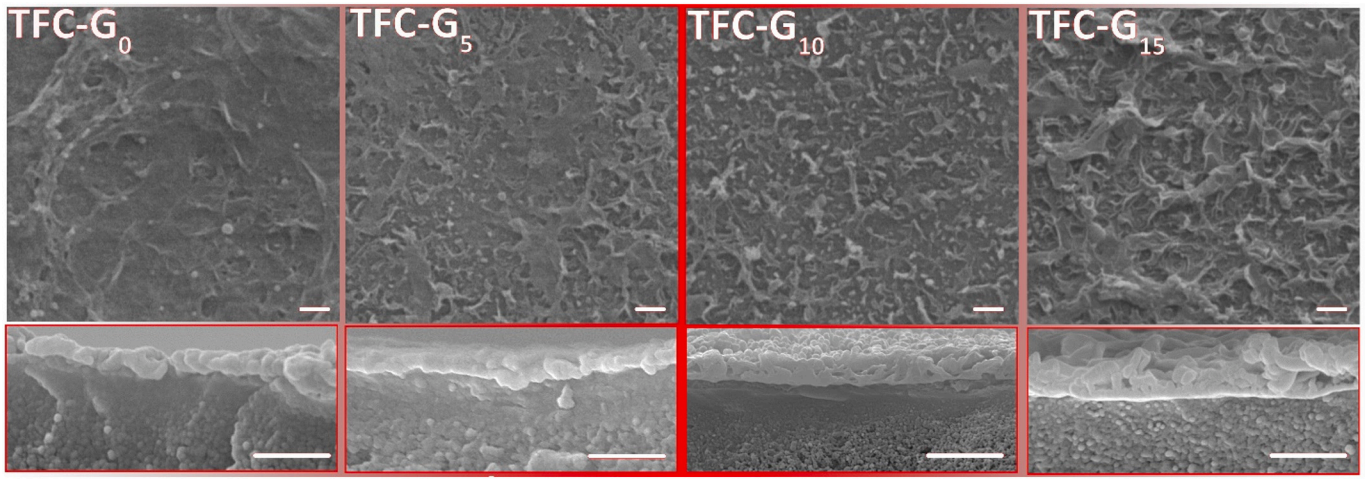

Fig. 5. Top surface and cross section morphology of TFC membranes (scale bars are 1 μm).

roughness (R_a) was investigated and shown in Fig. 6. The roughness is found to vary with the incorporation of PSf-g-PDMA graft copolymer and follows the order: TFC-G_{15}>TFC-G_{10}>TFC-G_5>TFC-G_0 (Table 2). This increasing order is consistent with the morphology analysis via SEM images.

Evaluation the intrinsic separation properties of PSf-g-PDMA modified membranes.

The intrinsic separation properties of the PSf-g-PDMA modified membranes in terms of water and salt permeability were examined in the dead-end RO set-up and results are presented in Table 3. In general, all the blended membranes have the higher A value than that of the pristine TFC membrane. In addition, there is a strong relation between the A value and concentration of PSf-g-PDMA copolymer. As can be seen by raising the copolymer concentration in membrane substrate from 0 to 10 wt%, the water permeance was increased from 1.21 for TFC-G_0 to 2.05 LMH/bar for TFC-G_{10}. This enhancement can be explained by the fact that the PA layer became rougher upon PSF-g-PDMA blending. The higher roughness of the resultant PA active layer on PSf/PSf-g-PDMA substrates enhances the surface area for water transport which improves the water permeance. The slight drop in the water permeance value of TFC-G_{15} membrane can be attributed to the larger transport resistance caused by the thicker PA layer. Compared to water permeance value, the salt rejection (R_s) shows an opposite trend. It decreases very slightly from 94.8% for TFG_0 membrane to 93.9% for the TFN-G_5 membrane and then declines obviously to 85.6% for TFC-G_{15} membrane.

In most FO studies, the ICP effects of a membrane substrate is expressed by the S value. Lower S value means a lower ICP effect of the membrane substrate and higher water flux in FO experiment. As the PSf-g-PDMA weight ratio rises from 0.0 to 10.0 wt%, the S value decreases from 1915 to 546 μm. This significant decrease in S value reflects a combination of effects including the increase of hydrophilicity and porosity, decrease in tortuosity and change in support morphology.

3.3. FO performance of PSf-g-PDMA blended membranes

The FO performance of the PSf-g-PDMA blended membranes was investigated in the lab-scale FO set-up for different draw solutions. Fig. 7 compares the FO performance using DI water and 1 M NaCl as feed and draw solution, respectively. As can be seen the water flux shows an up-and-down trend with PSf-g-PDMA copolymer loading in the membrane substrate from 0 to 15 wt%. Due to the low hydrophilicity, porosity and dense structure in bare PSf membrane substrate, its TFC membrane possesses a high structure parameter (S), which caused a lower water flux in the FO process. The enhancement in the water flux of copolymer-blended TFC membrane could be attributed to the improved membrane morphology with lower structure parameter, due to the enhanced porosity and hydrophilicity of the modified substrate. Moreover, the PA layer with rougher surface can enhance the water flux by providing large surface area for water transport [55]. However, the water flux enhancement was limited when the copolymer weight ratio was above 10 wt%. This could be ascribed to the formation of a thick PA selective layer on G_{15} membrane substrate. As can be seen TFC-G_{15} had the highest reverse salt flux among the composite membranes, which induces ICP, drops the osmotic driving force, and consequently results in a decline in water flux. The reverse salt flux shows a similar trend with that of the R_s data in the RO tests. The reverse salt fluxes increased from 1.77 gMH for TFC-G_0 to 2.49 gMH for TFC-G_{10}. Then, the reverse salt flux noticeably increased to 6.52 gMH for TFC-G_{15}. The selectivity (J_s/J_w) of the all TFC membranes was determined to better compare the performance of the different membranes and assess the osmotic process efficiency. In general, low reverse salt flux and high water flux are desired for a high-performance FO membrane [22]. As shown in Fig. 7b, the J_s/J_w value declined considerably for TFC-G_{10} membrane. Owing to the high reverse salt flux of TFC-G_{15}, the J_s/J_w dramatically increased when the PSf-g-PDMA weight ratio was above 15 wt%.

Table 2
PA layer thickness and roughness for different TFC membranes (R_a and R_q values are the average of measurements taken from a total of 3 random spots on sample surfaces).

Membranes	R_q (nm)	R_a (nm)	Thickness (nm)
TFC-G_0	83.5	62.7	285 ± 55
TFC-G_5	101.7	79.2	334 ± 47
TFC-G_{10}	118.1	91.8	401 ± 38
TFC-G_{15}	129.7	101.4	530 ± 43

Fig. 8 shows the FO performances of TFC-G0 and TFC-G10 in both FO and PRO modes as a function of draw and feed solutions pH. In general, a reversible dependence on pH was observed for TFC-G10 membrane. This pH-dependent permeability is attributed to the PDMA side chains which cover the membrane substrates pore surfaces. For the modified membrane the water flux in FO mode increases by changing the pH of the draw solution from 10.0 to 3.0. At acidic pH most of the –N(Me)2 groups are in positive form (–HN + (Me)2), which is able to increase the osmotic pressure difference across the selective layer as shown in Fig. 9a leading to an increase in water flux [56]. To prove this hypothesis, we measured the water flux of TFC-G10 in PRO mode using feed solutions at two different pH values (3.0 and 10.0). In this case, the water flux for the pH 10.0 feed solution is higher than for pH 3.0. In PRO mode, the support layer is facing the feed solution, causing protonation of DMA groups in pH 3.0. This leads to a decline in the effective pore size, osmotic pressure difference and consequently the water flux. The reversibility of this water flux pH dependency for TFC-G10 in FO mode was investigated by consecutively changing the pH of the draw solution between 3.0 and 10.0. The results are shown in Fig. 8b, where it can be seen that the TFC-G10 could retain its stimuli-responsive behavior after several pH 3 → 10 → 3 cycles while the water flux was relatively stable during these cycles.

Table 4 compare the porosity and hydrophilicity of the different polymer modified substrates and FO performances of resultant TFC

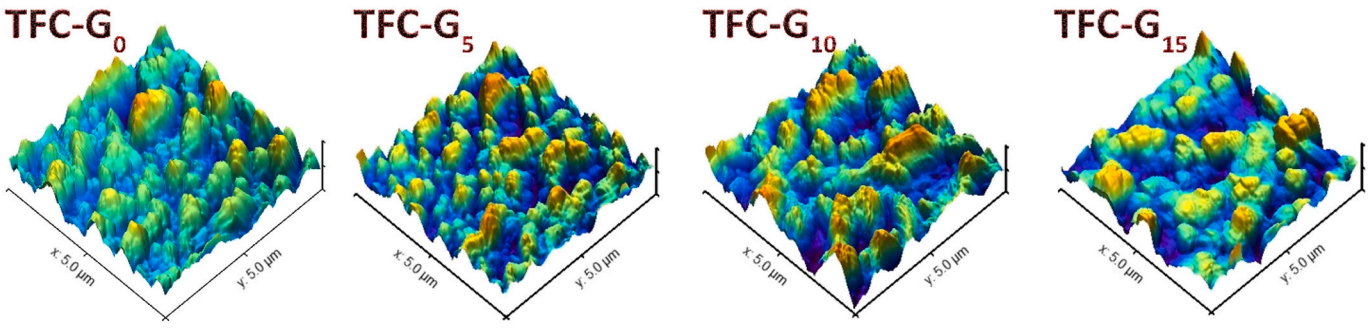

Fig. 6. AFM images measured by AFM tapping mode analysis.

Table 3
The intrinsic separation properties as well as structure parameters of TFC membranes (results are an average of three different membrane coupons).

TFC Membranes	Water permeance A (LMH/bar)	Salt rejection R_s (%)	Salt flux B (LMH)	S (μm)
TFC-G_0	1.21 ± 11	94.8 ± 0.31	0.34 ± 0.04	1915.2 ± 137
TFC-G_5	1.73 ± 0.08	93.9 ± 0.45	0.56 ± 0.07	816.7 ± 99
TFC-G_{10}	2.05 ± 0.09	94.3 ± 0.50	0.61 ± 0.08	546.5 ± 44
TFC-G_{15}	1.86 ± 0.06	85.6 ± 0.54	1.56 ± 0.23	657 ± 110

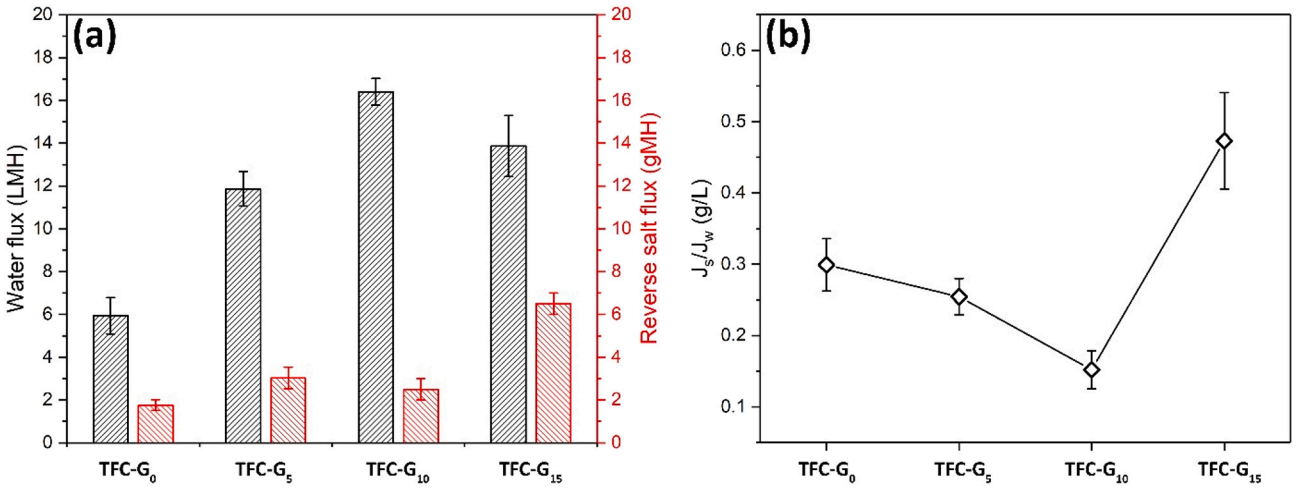

Fig. 7. FO performances of TFC membranes using DI water as feed solution and 1 M NaCl aas draw solution, (a) water flux and reverse salt flux, and (b) specific reverse salt flux in FO mode (results are an average of three different membrane coupons).

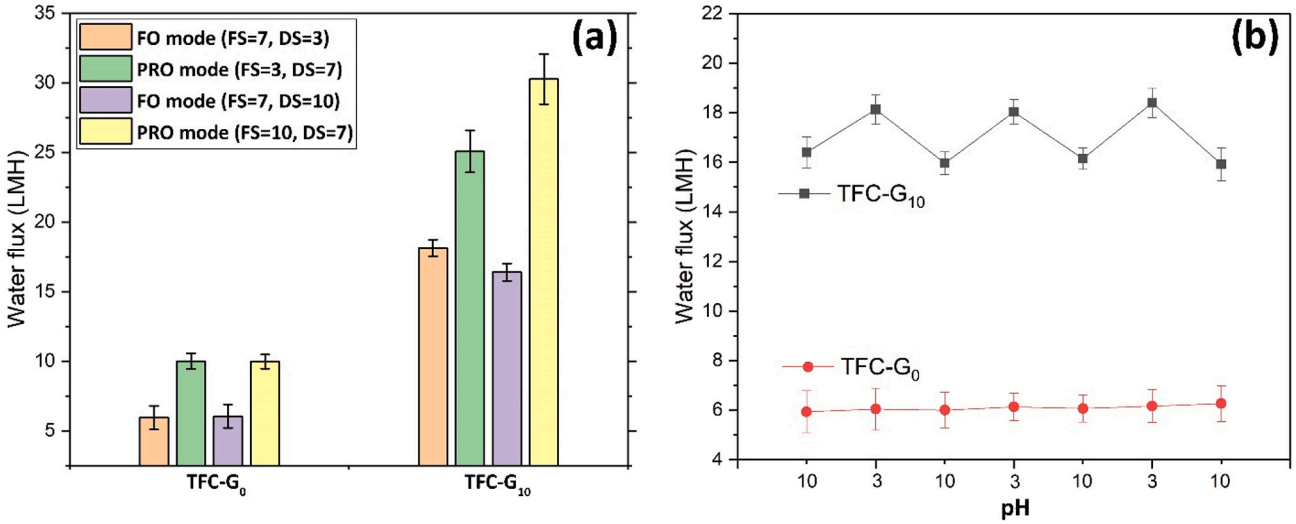

Fig. 8. (a) Water flux of TFC-G_0 and TFC-G_{10} membranes in FO and PRO modes, (b) water flux reversibility test of TFC-G_0 and TFC-G_{10} membranes in FO mode (results are an average of three different membrane coupons).

membranes in this study and those reported in the literatures. As can be seen, modification of membrane substrate with PSf-g-PDMA graft copolymer could improve the FO water flux of original composite membrane up to 178%. Compared to other polymer modified TFC membranes, the TFC-G_{10} with the lowest weight ratio of graft copolymer presented an outstanding improvement in water flux of original TFC membrane, while the other TFC membranes required higher weight ratio of modifiers (even 50%) to obtain the same level increase in water flux. Moreover, G_{10} substrate and its resultant TFC-G_{10} membrane shows a pH-dependence water flux in UF and FO process, while other membranes modified by traditional modifiers usually have non-adjustable water permeability. In addition, membrane selectivity was improved after introduction PSf-g-PDMA graft copolymer into the membrane substrates, which establishing again that the blending of PSf-

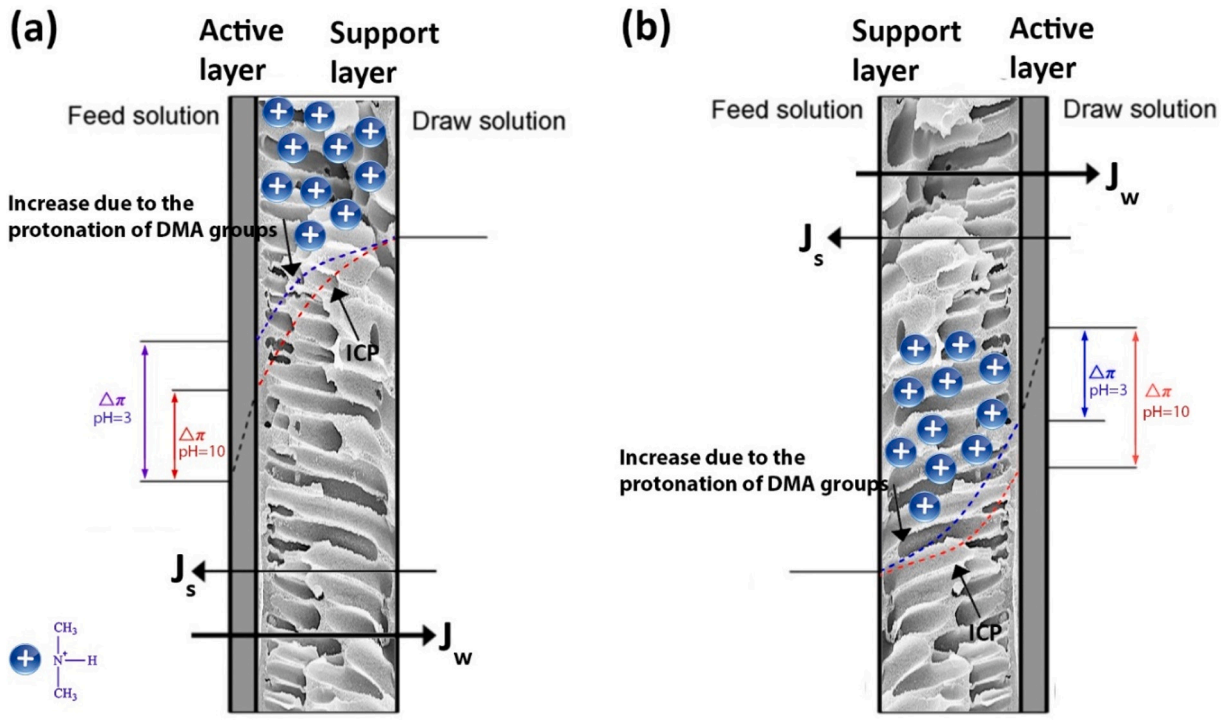

Fig. 9. Effect of pH of feed and draw solutions on effective osmotic pressure in (a) FO and (b) PRO modes.

Table 4
Performances of recent TFC membranes with different polymer modified substrates.

Membrane subtract		PES-co-sPPSU	CPSF65	Sub-25	PSf-PEG	TFC-G_{10}
Substrate		PES	PSf	PSf	PSf	PSf
Modifier		PES-co-sPPSU	CPSf	BPSH10	PEG-PSf	PSf-PDMA
Weight ratio (%)		50	100	25	100	10
Porosity (%)	Original	80.3	70.1	72.9	73.7	77.3
	Modified	84.9	81.2	80.2	80.4	82.1
WCA (°)	Original	77.3	65.0	82.5	85.1	80.1
	Modified	57.3	51.0	56.6	12.1	64.5
J_w (LMH)	Original	10.5	10.5	20.2	30.1	5.9
	Modified	21.0	17.9	40.9	35.4	16.4
	Incr. (%)	100	70	102	18	178
J_s (gMH)	Original	3.1	1.7	3.4	4.0	1.8
	Modified	2.2	2.3	9.3	7.4	2.5
S (μm)	Original	963.0	–	495.0	453.0	1915
	Modified	324.0	–	186.0	412.0	546
J_s/J_w (g/L)	Original	0.29	0.16	0.17	0.13	0.30
	Modified	0.11	0.13	0.23	0.21	0.15
Test condition	Feed	DI water	DI water	DI water	DI water	DI water
	Draw	2 M NaCl	1 M MgC_2	2 M NaCl	1 M NaCl	1 M NaCl
	Mode	FO	FO	FO	PRO	FO
Adjustable water flux		No	No	No	No	Yes
Reference		[57]	[35]	[58]	[59]	This work

g-PDMA copolymer with PSf substrate could be a promising methodology to enhance the FO performance of the resultant TFC membranes.

4. Conclusion

For the first time, hydrophilic PSf-g-PDMA copolymer was synthesized and subsequently blended in PSf support layer for the fabrication of pH-responsive TFC-FO membranes. The effects of PSf-g-PDMA weight ratio on the physicochemical properties and water permeability of the resultant support layers and the TFC membranes were studied. The PWP measurements of G_{10} support layer revealed that the water flux in basic feed solution is higher than acidic feed solution due to the swollen conformation of PDMA chain and consequently close state of pores in acidic solution. Compared with the bare PSf based TFC membrane, PSF-g-PDMA blended based TFC membranes show the higher water flux (up to 16.4 LMH in the FO mode) without adversely affecting on selectivity. This enhancement in water flux might be ascribed to the following characteristics of PSf-g-PDMA modified substrate: (1) high hydrophilicity, (2) high porosity, (3) minimal tortuosity, which contribute to a low structure parameter. More importantly, the TFC-G_{10} like its substrate shows a reversible pH-dependent water flux in FO process. Modification of the membrane substrate by PSf-g-PDMA copolymer with pH-responsive switchable behavior may provide valuable insight into the fabrication of high performance TFC membranes for FO and other commercial applications.

Declaration of competing interest

The authors declare that they have no known competing financial interests or personal relationships that could have appeared to influence the work reported in this paper.

Acknowledgment

We would like to acknowledge the University of Tehran for received financial and instrumental support.

Appendix A. Supplementary data

Supplementary data to this article can be found online at https://doi.org/10.1016/j.desal.2020.114731.

References

[1] A. Subramani, J.G. Jacangelo, Emerging desalination technologies for water treatment: a critical review, Water Res. 75 (2015) 164–187, https://doi.org/10.1016/j.watres.2015.02.032.
[2] B. Mi, M. Elimelech, Organic fouling of forward osmosis membranes: fouling reversibility and cleaning without chemical reagents, J. Memb. Sci. 348 (2010) 337–345, https://doi.org/10.1016/j.memsci.2009.11.021.
[3] A. Shakeri, H. Mighani, N. Salari, H. Salehi, Surface modification of forward osmosis membrane using polyoxometalate based open frameworks for hydrophilicity and water flux improvement, J. Water Process Eng. 29 (2019) 100762, https://doi.org/10.1016/j.jwpe.2019.02.002.
[4] J.B. Zimmerman, J.R. Mihelcic, J. Smith, Global stressors on water quality and quantity, Environ. Sci. Technol. 42 (2008) 4247–4254, https://doi.org/10.1021/es0871457.
[5] J.R. Werber, C.O. Osuji, M. Elimelech, Erratum: materials for next-generation desalination and water purification membranes, Nat. Rev. Mater. 16037 (2016), https://doi.org/10.1038/natrevmats.2016.37.
[6] Y. Zhao, X. Wang, Y. Ren, D. Pei, Mesh-embedded polysulfone/sulfonated polysulfone supported thin film composite membranes for forward osmosis, ACS Appl. Mater. Interfaces 7b15309 (2018), https://doi.org/10.1021/acsami.7b15309 acsami.
[7] A. Shakeri, H. Salehi, F. Ghorbani, M. Amini, H. Naslhajian, Polyoxometalate based thin film nanocomposite forward osmosis membrane: Superhydrophilic, antifouling, and high water permeable, J. Colloid Interface Sci. 536 (2019) 328–338, https://doi.org/10.1016/j.jcis.2018.10.069.
[8] H. Salehi, A. Shakeri, H. Naslhajian, M. Amini, High-flux thin film nanocomposite forward osmosis membrane incorporated with blue lemon polyoxometalate based open-framework, J. Polym. Res. 26 (2019), https://doi.org/10.1007/s10965-019-1713-9.
[9] G. Chen, R. Liu, H.K. Shon, Y. Wang, J. Song, X.M. Li, T. He, Open porous hydrophilic supported thin-film composite forward osmosis membrane via co-casting for treatment of high-salinity wastewater, Desalination. 405 (2017) 76–84, https://doi.org/10.1016/j.desal.2016.12.004.
[10] G. Han, T.S. Chung, M. Toriida, S. Tamai, Thin-film composite forward osmosis membranes with novel hydrophilic supports for desalination, J. Memb. Sci. 423–424 (2012) 543–555, https://doi.org/10.1016/j.memsci.2012.09.005.
[11] G. Han, S. Zhang, X. Li, N. Widjojo, T.S. Chung, Thin film composite forward osmosis membranes based on polydopamine modified polysulfone substrates with enhancements in both water flux and salt rejection, Chem. Eng. Sci. 80 (2012) 219–231, https://doi.org/10.1016/j.ces.2012.05.033.
[12] S. Zhao, L. Zou, C.Y. Tang, D. Mulcahy, Recent developments in forward osmosis: opportunities and challenges, J. Memb. Sci. 396 (2012) 1–21, https://doi.org/10.1016/j.memsci.2011.12.023.
[13] A. Tiraferri, Y. Kang, E.P. Giannelis, M. Elimelech, Highly hydrophilic thin-film composite forward osmosis membranes functionalized with surface-tailored nanoparticles, ACS Appl. Mater. Interfaces 4 (2012) 5044–5053, https://doi.org/10.1021/am301532g.
[14] D. Emadzadeh, W.J. Lau, M. Rahbari-Sisakht, H. Ilbeygi, D. Rana, T. Matsuura, A.F. Ismail, Synthesis, modification and optimization of titanate nanotubes-polyamide thin film nanocomposite (TFN) membrane for forward osmosis (FO) application, Chem. Eng. J. 281 (2015) 243–251, https://doi.org/10.1016/j.cej.2015.06.035.
[15] N. Ma, J. Wei, R. Liao, C.Y. Tang, Zeolite-polyamide thin film nanocomposite membranes: towards enhanced performance for forward osmosis, J. Memb. Sci. 405–406 (2012) 149–157, https://doi.org/10.1016/j.memsci.2012.03.002.
[16] N. Ma, J. Wei, S. Qi, Y. Zhao, Y. Gao, C.Y. Tang, Nanocomposite substrates for controlling internal concentration polarization in forward osmosis membranes, J. Memb. Sci. 441 (2013) 54–62, https://doi.org/10.1016/j.memsci.2013.04.004.
[17] J. Wei, C. Qiu, C.Y. Tang, R. Wang, A.G. Fane, Synthesis and characterization of flat-sheet thin film composite forward osmosis membranes, J. Memb. Sci. 372 (2011) 292–302, https://doi.org/10.1016/j.memsci.2011.02.013.
[18] N. Widjojo, T.-S. Chung, M. Weber, C. Maletzko, V. Warzelhan, A sulfonated polyphenylenesulfone (sPPSU) as the supporting substrate in thin film composite (TFC) membranes with enhanced performance for forward osmosis (FO), Chem. Eng. J. 220 (2013) 15–23, https://doi.org/10.1016/j.cej.2013.01.007.
[19] Q. Liu, J. Li, Z. Zhou, J. Xie, J.Y. Lee, Hydrophilic mineral coating of membrane substrate for reducing internal concentration polarization (ICP) in forward osmosis, Sci. Rep. 6 (2016) 19593, https://doi.org/10.1038/srep19593.
[20] M. Rastgar, A. Shakeri, A. Bozorg, H. Salehi, V. Saadattalab, Impact of nanoparticles surface characteristics on pore structure and performance of forward osmosis membranes, Desalination. 421 (2017) 179–189, https://doi.org/10.1016/j.desal.2017.01.040.
[21] X. Fan, Y. Liu, X. Quan, S. Chen, Highly permeable thin-film composite forward osmosis membrane based on carbon nanotube hollow fiber scaffold with electrically enhanced fouling resistance, Environ. Sci. Technol. 7b05341 (2018), https://doi.org/10.1021/acs.est.7b05341 acs.est.
[22] X. Liu, H.Y. Ng, Fabrication of layered silica-polysulfone mixed matrix substrate membrane for enhancing performance of thin-film composite forward osmosis membrane, J. Memb. Sci. 481 (2015) 148–163, https://doi.org/10.1016/j.memsci.2015.02.012.
[23] X. Zhang, L. Shen, C.Y. Guan, C.X. Liu, W.Z. Lang, Y. Wang, Construction of SiO2@MWNTs incorporated PVDF substrate for reducing internal concentration polarization in forward osmosis, J. Memb. Sci. 564 (2018) 328–341, https://doi.org/10.1016/j.memsci.2018.07.043.
[24] H. Salehi, A. Shakeri, M. Rastgar, Carboxylic polyethersulfone: a novel pH-responsive modifier in support layer of forward osmosis membrane, J. Memb. Sci. 548 (2018) 641–653, https://doi.org/10.1016/j.memsci.2017.10.044.
[25] J. Li, Q. Liu, X. Li, Y. Liu, J. Xie, Template-assisted fabrication of thin-film composite forward-osmosis membrane with controllable internal concentration polarization, Ind. Eng. Chem. Res. 55 (2016) 5327–5334, https://doi.org/10.1021/acs.iecr.6b00874.
[26] W. Kuang, Z. Liu, G. Kang, D. Liu, M. Zhou, Y. Cao, Thin film composite forward osmosis membranes with poly(2-hydroxyethyl methacrylate) grafted nano-TiO2 as additive in substrate, J. Appl. Polym. Sci. 133 (2016) 1–10, https://doi.org/10.1002/app.43719.
[27] M. Tian, Y.N. Wang, R. Wang, A.G. Fane, Synthesis and characterization of thin film nanocomposite forward osmosis membranes supported by silica nanoparticle incorporated nanofibrous substrate, Desalination. 401 (2017) 142–150, https://doi.org/10.1016/j.desal.2016.04.003.
[28] X. Song, Z. Liu, D.D. Sun, Nano gives the answer: breaking the bottleneck of internal concentration polarization with a nanofiber composite forward osmosis membrane for a high water production rate, Adv. Mater. 23 (2011) 3256–3260, https://doi.org/10.1002/adma.201100510.
[29] J. Zhou, H.-L. He, F. Sun, Y. Su, H.-Y. Yu, J.-S. Gu, Structural parameters reduction in polyamide forward osmosis membranes via click modification of the polysulfone support, Colloids Surfaces A Physicochem. Eng. Asp. 585 (2020) 124082, https://doi.org/10.1016/J.COLSURFA.2019.124082.
[30] L. Huang, J.T. Arena, J.R. McCutcheon, Surface modified PVDF nanofiber supported thin film composite membranes for forward osmosis, J. Memb. Sci. 499 (2016) 352–360, https://doi.org/10.1016/j.memsci.2015.10.030.
[31] P. Lu, S. Liang, T. Zhou, X. Mei, Y. Zhang, C. Zhang, A. Umar, Q. Wang, Layered double hydroxide/graphene oxide hybrid incorporated polysulfone substrate for thin-film nanocomposite forward osmosis membranes, RSC Adv. 6 (2016) 56599–56609, https://doi.org/10.1039/C6RA10080E.
[32] P. Lu, W. Li, S. Yang, Y. Wei, Z. Zhang, Y. Li, Layered double hydroxides (LDHs) as novel macropore-templates: the importance of porous structures for forward osmosis desalination, J. Memb. Sci. 585 (2019) 175–183, https://doi.org/10.1016/j.memsci.2019.05.045.
[33] X. Song, L. Wang, L. Mao, Z. Wang, Nanocomposite membrane with different carbon nanotubes location for nanofiltration and forward osmosis applications, ACS Sustain. Chem. Eng. 4 (2016) 2990–2997, https://doi.org/10.1021/acssuschemeng.5b01575.
[34] J. Xu, P. Li, M. Jiao, B. Shan, C. Gao, Effect of molecular configuration of additives on the membrane structure and water transport performance for forward osmosis, ACS Sustain. Chem. Eng. 4 (2016) 4433–4441, https://doi.org/10.1021/acssuschemeng.6b01039.
[35] Y.H. Cho, J. Han, S. Han, M.D. Guiver, H.B. Park, Polyamide thin-film composite membranes based on carboxylated polysulfone microporous support membranes for forward osmosis, J. Memb. Sci. 445 (2013) 220–227, https://doi.org/10.1016/j.memsci.2013.06.003.
[36] C. Zhao, S. Nie, M. Tang, S. Sun, Polymeric pH-sensitive membranes—a review, Prog. Polym. Sci. 36 (2011) 1499–1520, https://doi.org/10.1016/j.progpolymsci.2011.05.004.
[37] L. Miao, Y. Tu, Y. Yang, S. Lin, J. Hu, M. Zhang, Y. Li, F. Li, Y. Mo, Robust stimuli-responsive membranes prepared from a blend of polysulfone and a graft copolymer bearing binary side chains with thermo- and pH-responsive switching behavior, Chem. - A Eur. J. 23 (2017) 7737–7747, https://doi.org/10.1002/chem.201605263.
[38] D. Wandera, S.R. Wickramasinghe, S.M. Husson, Stimuli-responsive membranes, J. Memb. Sci. 357 (2010) 6–35, https://doi.org/10.1016/j.memsci.2010.03.046.
[39] T. Luo, S. Lin, R. Xie, X.-J. Ju, Z. Liu, W. Wang, C.-L. Mou, C. Zhao, Q. Chen, L.-Y. Chu, pH-responsive poly(ether sulfone) composite membranes blended with amphiphilic polystyrene-block-poly(acrylic acid) copolymers, J. Memb. Sci. 450 (2014) 162–173, https://doi.org/10.1016/J.MEMSCI.2013.09.002.
[40] L. Liu, C. Tong, Y. He, Y. Zhao, C. Lü, Enhanced properties of quaternized graphenes reinforced polysulfone based composite anion exchange membranes for alkaline fuel cell, J. Memb. Sci. 487 (2015) 99–108, https://doi.org/10.1016/j.memsci.2015.03.077.
[41] Y. Yang, L. Miao, J. Hu, G. Liu, Y. Tu, S. Lin, F. Liu, F. Li, Y. Wu, G. Zhang, H. Zou,

Hydrophilization of polysulfone membranes using a binary graft copolymer, J. Mater. Chem. A 2 (2014) 10410–10423, https://doi.org/10.1039/C4TA01481B.
[42] C. Hou, S. Lin, F. Liu, J. Hu, G. Zhang, G. Liu, Y. Tu, H. Zou, H. Luo, Synthesis of poly(2-hydroxyethyl methacrylate) end-capped with asymmetric functional groups via atom transfer radical polymerization, New J. Chem. 38 (2014) 2538, https://doi.org/10.1039/c3nj01398g.
[43] Z. Ge, D. Wang, Y. Zhou, H. Liu, S. Liu, Synthesis of organic/inorganic hybrid quatrefoil-shaped star-cyclic polymer containing a polyhedral Oligomeric silsesquioxane core, Macromolecules. 42 (2009) 2903–2910, https://doi.org/10.1021/ma802585k.
[44] W. Ding, Y. Li, M. Bao, J. Zhang, C. Zhang, J. Lu, Highly permeable and stable forward osmosis (FO) membrane based on the incorporation of Al2O3 nanoparticles into both substrate and polyamide active layer, RSC Adv. 7 (2017) 40311–40320, https://doi.org/10.1039/C7RA04046F.
[45] Z. Zhou, J.Y. Lee, T.S. Chung, Thin film composite forward-osmosis membranes with enhanced internal osmotic pressure for internal concentration polarization reduction, Chem. Eng. J. 249 (2014) 236–245, https://doi.org/10.1016/j.cej.2014.03.049.
[46] G.R. Xu, J.M. Xu, H.J. Feng, H.L. Zhao, S.B. Wu, Tailoring structures and performance of polyamide thin film composite (PA-TFC) desalination membranes via sublayers adjustment-a review, Desalination. 417 (2017) 19–35, https://doi.org/10.1016/j.desal.2017.05.011.
[47] M. Corvilain, C. Klaysom, A. Szymczyk, I.F.J. Vankelecom, Formation mechanism of sPEEK hydrophilized PES supports for forward osmosis, Desalination. 419 (2017) 29–38, https://doi.org/10.1016/J.DESAL.2017.05.037.
[48] G.S. Lai, M.H.M. Yusob, W.J. Lau, R.J. Gohari, D. Emadzadeh, A.F. Ismail, P.S. Goh, A.M. Isloor, M.R.D. Arzhandi, Novel mixed matrix membranes incorporated with dual-nanofillers for enhanced oil-water separation, Sep. Purif. Technol. 178 (2017) 113–121, https://doi.org/10.1016/j.seppur.2017.01.033.
[49] Z. Yi, L.-P. Zhu, Y.-F. Zhao, Z.-B. Wang, B.-K. Zhu, Y.-Y. Xu, Effects of coagulant pH and ion strength on the dehydration and self-assembly of poly(N, N-dimethylamino-2-ethyl methacrylate) chains in the preparation of stimuli-responsive polyethersulfone blend membranes, J. Memb. Sci. 463 (2014) 49–57, https://doi.org/10.1016/j.memsci.2014.03.041.
[50] A. Rahimpour, S.S. Madaeni, S. Ghorbani, A. Shockravi, Y. Mansourpanah, The influence of sulfonated polyethersulfone (SPES) on surface nano-morphology and performance of polyethersulfone (PES) membrane, Appl. Surf. Sci. 256 (2010) 1825–1831, https://doi.org/10.1016/j.apsusc.2009.10.014.
[51] T. Tavangar, A. Hemmati, M. Karimi, F. Zokaee Ashtiani, Layer-by-layer assembly of graphene oxide (GO) on sulfonated polyethersulfone (SPES) substrate for effective dye removal, Polym. Bull. 76 (2019) 35–52, https://doi.org/10.1007/s00289-018-2357-3.
[52] X. Zhang, L. Shen, W.Z. Lang, Y. Wang, Improved performance of thin-film composite membrane with PVDF/PFSA substrate for forward osmosis process, J. Memb. Sci. 535 (2017) 188–199, https://doi.org/10.1016/j.memsci.2017.04.038.
[53] K. Zheng, S. Zhou, X. Zhou, A low-cost and high-performance thin-film composite forward osmosis membrane based on an SPSU/PVC substrate, Sci. Rep. 8 (2018) 10022, https://doi.org/10.1038/s41598-018-28436-4.
[54] X. Li, K.Y. Wang, B. Helmer, T.S. Chung, Thin-film composite membranes and formation mechanism of thin-film layers on hydrophilic cellulose acetate propionate substrates for forward osmosis processes, Ind. Eng. Chem. Res. 51 (2012) 10039–10050, https://doi.org/10.1021/ie2027052.
[55] W.J. Lau, A.F. Ismail, P.S. Goh, N. Hilal, B.S. Ooi, Characterization methods of thin film composite nanofiltration membranes, Sep. Purif. Rev. 44 (2015) 135–156, https://doi.org/10.1080/15422119.2014.882355.
[56] Y. Cai, W. Shen, R. Wang, W.B. Krantz, A.G. Fane, X. Hu, CO2 switchable dual responsive polymers as draw solutes for forward osmosis desalination, Chem. Commun. 49 (2013) 8377, https://doi.org/10.1039/c3cc43289k.
[57] N. Widjojo, T.S. Chung, M. Weber, C. Maletzko, V. Warzelhan, The role of sulphonated polymer and macrovoid-free structure in the support layer for thin-film composite (TFC) forward osmosis (FO) membranes, J. Memb. Sci. 383 (2011) 214–223, https://doi.org/10.1016/j.memsci.2011.08.041.
[58] X. Zhang, J. Tian, Z. Ren, W. Shi, Z. Zhang, Y. Xu, S. Gao, F. Cui, High performance thin-film composite (TFC) forward osmosis (FO) membrane fabricated on novel hydrophilic disulfonated poly(arylene ether sulfone) multiblock copolymer/polysulfone substrate, J. Memb. Sci. 520 (2016) 529–539, https://doi.org/10.1016/j.memsci.2016.08.005.
[59] X. An, Y. Hu, N. Wang, T. Wang, Z. Liu, Breaking the permeability–selectivity trade-off in thin-film composite polyamide membranes with a PEG-b-PSF-b-PEG block copolymer ultrafiltration membrane support through post-annealing treatment, NPG Asia Mater. 11 (2019) 1–12, https://doi.org/10.1038/s41427-019-0114-1.